Multidecadal Evolution of the Turbidity Maximum Zone in a Macrotidal River Under Climate and Anthropogenic Pressures

I Jalón-rojas, Y M Dijkstra, H M Schuttelaars, R L Brouwer, Sabine Schmidt, A Sottolichio

Multi-Decadal Evolution of the Turbidity Maximum Zone in a Macrotidal River under Climate and Anthropogenic Pressures

I. Jalón-Rojas[1,2], Y.M. Dijkstra[3], H.M. Schuttelaars[3], R.L. Brouwer[3,4], S.Schmidt[1] and A. Sottolichio[1]

[1]UMR5805 EPOC, CNRS, OASU, Université de Bordeaux, Pessac, France

[2]The Sino-Australian Research Centre for Coastal Management, School of Science, UNSW Canberra, Canberra, Australia

[3]Delft Institute of Applied Mathematics, Delft University of Technology, Delft, Netherlands

[4]Flanders Hydraulics Research, Antwerp, Belgium

Corresponding author: Isabel Jalón-Rojas (isabel.jalon-rojas@u-bordeaux.fr; ijalonrojas@gmail.com)

Key Points:

- Morphological and hydrological changes contributed to the upstream shift of the turbidity maximum zone over the last six decades.
- This shift is explained by an enhanced sediment import driven by the external M4 tide, tidal return flow, and spatial settling lag effects.
- Climate-induced morphological changes were the main pressure inducing the displacement and intensification of the turbidity maximum zone.

This article has been accepted for publication and undergone full peer review but has not been through the copyediting, typesetting, pagination and proofreading process, which may lead to differences between this version and the Version of Record. Please cite this article as doi: 10.1029/2020JC016273.

Abstract

Climate and human pressures can influence the evolution of estuarine sediment dynamics concurrently, but the understanding and quantification of their cause-effect relationships are still challenging due to the occurrence of complex hydro-morpho-sedimentary feedbacks. The Garonne Tidal River (GTR, upper Gironde Estuary, France) is a clear example of a system stressed by both anthropogenic and climate change, as it has been subject to decreasing river discharges, natural morphological changes, and gravel extraction. To understand the relative effect of each hydrological and geomorphological pressure on the turbidity maximum zone (TMZ), the sediment dynamics in the GTR over the last six decades was evaluated using the width-averaged idealized iFlow model. Model results show a gradual increase in tidal amplitude and currents over the decades that has led to the upstream shift of the landward sediment-transport capacity components (external M4 tide, spatial settling lag, and tidal return flow). The upstream displacement of the TMZ between the 1950s and the 2010s was estimated to be at least 19 km, of which about 3/4 was induced by geomorphological changes and 1/4 by hydrological changes. Concerning the geomorphological changes, the natural evolution of the lower Gironde morphology was the main pressure inducing the displacement of the TMZ in the GTR. Anthropogenic and natural changes in morphology and bed roughness in the GTR itself also contributed to this evolution. The natural geomorphological changes were, in turn, probably promoted by the evolution of sediment dynamics, so this study reveals the closed circle that governs the intensification of the TMZ.

Plain Language Summary

According to local managers, the Garonne Tidal River has experienced an increase of sediment concentration between the 1960s and the 2010s. During this period, the tidal river was subject to decreasing river discharges, morphological changes controlled by natural boundary conditions, and gravel extraction. To test this hypothesis and to better understand the influence of climate and human pressures on the estuarine sediment dynamics, this study evaluates the evolution of sediment transport patterns in the Garonne Tidal River over the last six decades. In the absence of historical observations of sediment concentration, we applied the idealized model iFlow to different scenarios of river discharge and morphology. Model results show a gradual increase in the landward transport of sediment over the decades. The natural evolution of the morphology was the main pressure inducing the upstream shift of the maximum concentrations. The model uses simplified descriptions of physical mechanisms, allowing for a systematic analysis of the underlying physical processes that contributed to the multidecadal evolution of sediment transport.

1 Introduction

Estuaries are dynamically complex systems, characterized by a strong interaction between hydrodynamics, sediment transport, and morphodynamics. Both climate change/variability and human activities can strongly influence this interaction, possibly resulting in complex hydro-morpho-sedimentary feedbacks (Winterwerp and Wang, 2013; Jalón-Rojas et al., 2018). These feedbacks can cause variations in sediment transport and trapping phenomena, such as the turbidity maximum zone (TMZ), over both long and short periods; it can therefore impact estuarine ecosystems, water quality, socioeconomic value, and natural-resource

management (Little et al., 2017). Identifying and distinguishing the effects of climate and human pressures on the medium- and long-term evolution of sediment dynamics is critical to understanding trends and predicting the evolution of estuarine environments, but challenging due to the coexistence of various interactive processes impacting sediment transport and trapping at different temporal and spatial scales (Gallop et al., 2015).

Recent research efforts have investigated the impact of human-induced morphological changes on sediment dynamics. In tide-dominated estuaries, morphological changes can significantly alter the amplification (or damping) and the asymmetry of tidal waves induced by non-linear effects as they propagate landward (e.g., Friedrichs & Aubrey, 1988, Godin, 1999; Savenije et al., 2008; Guo et al., 2015; Talke et al., 2020). This can modify the sediment-transport asymmetry (imbalance between flood and ebb sediment transport), which can in turn alter the morphological evolution, and so on. For example, several studies on convergent, anthropized estuaries have demonstrated that channel deepening (e.g., Jay et al., 2011; Cai et al., 2012; Winterwerp & Wang, 2013; de Jonge et al., 2014; van Maren et al., 2015; Familkhalili and Talke, 2016; Ralston et al., 2018; Ralston and Geyer, 2019; Dijkstra et al., 2019c) and shortening (e.g., Chernetsky et al., 2010; Schuttelaars et al., 2013) can lead to increased tidal range and flood-dominance, which can favour a deeper penetration of tides up-estuary and the landward net transport of sediments. It should be noted that channel deepening can also decrease the flow velocity and the bed shear stress at the TMZ location, resulting in a reduction of suspension and therefore in lower sediment concentrations (e.g. Van Kessel et al., 2008; Dijskstra et al., 2019a). Apart from channel deepening, also channel narrowing can increase tidal range (e.g., Loire and Ems estuaries, Winterwerp et al., 2013) or decrease it (tidal choking, e.g., Yangshan Harbour, Guo et al., 2018; Yalu River Estuary, Cheng et al., 2020), depending on the balance between the enhanced effects of channel convergence and friction. As recently reported by several studies (van Maren et al., 2016; Burchard et al. 2018; Grasso and Le Hir, 2019; Dijkstra et al., 2019b; 2019c), the impact of human interventions on sediment dynamics depends on the dominant physical transport mechanisms, and the sensitivity of these mechanisms to the interventions, which may vary from estuary to estuary. This implies that observable indicators (e.g. tidal range, convergence number) might not be able to predict the effect of human interventions on sediment patterns, and system-specific modelling of individual estuaries is necessary (Dijkstra et al., 2019b).

Climate-induced changes in hydrological, atmospheric, and sea-level forcings also impact the physical processes and trigger TMZ shifts and morphological changes. For example, changes in river discharge can modify the contribution of river-induced residual currents to sediment transport (e.g., Brouwer et al., 2018), which can displace the natural position of the TMZ (Jalón-Rojas et al., 2015). Recent studies suggest that predicted climate-induced changes in river discharge will have a larger effect on sediment dynamics than sea-level rise (Costa et al., 2018; van Maanen and Sottolichio, 2018). Estuarine morphology therefore evolves because of the changes in natural boundary conditions, but the feedback response of these natural morphological changes on hydro-sedimentary dynamics has scarcely been studied (Moore et al., 2009). In addition, our knowledge of the response of estuarine sediment dynamics to the concurrent effects of climate and human forcing is still very limited, and further research on the underlying physical processes is required.

In view of the foregoing, the aim of this paper is to understand and estimate the relative effects of climate- and human-induced geomorphological and hydrological changes on the

physical mechanisms that dominate sediment dynamics in the Garonne Tidal River (GTR) and to evaluate the consequences for the TMZ. For this purpose, we apply the width- averaged idealized iFlow model to different morphological and hydrological scenarios. The GTR (upper Gironde Estuary, SW France, Fig. 1.a) is an ideal example of a system stressed by climate- and human-induced changes during the past decades. Jalón-Rojas et al. (2018) quantified the influence of these pressures on the multi-decadal evolution of the tidal range and tidal vertical asymmetry, and suggested the existence of feedback mechanisms that may affect the evolution of sediment dynamics and, in particular, the TMZ. These pressures are:

– Climate change and, to a lesser extent, the increase in surface irrigation have decreased the freshwater input to the estuary (Boé et al., 2009): the Garonne river's mean annual discharge has decreased from 650 m^3/s in the 1950s to 445 m^3/s currently; dry periods are now longer and large river floods are becoming less frequent (Jalón-Rojas et al., 2015). These changes may have enhanced the concentration, persistence and upstream displacement of the turbidity maximum (Jalón-Rojas et al., 2015) and also the tidal range and vertical tidal asymmetry (Jalón-Rojas et al., 2018).

– The estuary has undergone moderate climate-induced bathymetric changes. Despite the limited number of morphological data, Sottolichio et al. (2013) revealed a shift in the preferential area of sedimentation from the lower to the upper estuary between 1970 and 1994, probably related to the upstream shift of the TMZ. Natural morphological changes contributed in turn to the increase in tidal range and relative phase of the vertical tide defined by $2\Phi M2-\Phi M4$, both up to 12–15% between 1953 and 2014 (e.g. from 4.9 m and 66º to 5.6 m and 77º in average at Bordeaux Harbour; Jalón-Rojas et al., 2018).

– Gravel extraction between the 1960s and the 1980s has deepened several sections (Fig. 1.b), eliminated intertidal zones, and led to smoother beds (Castaing et al., 2006). As a consequence, the increase of tidal range and relative phase of the vertical tide was doubled in these sections compared to the lower reaches during this period (Jalón-Rojas et al., 2018).

– Displacements of the turbidity maximum and its associated mobile mud modify bottom roughness and therefore tidal range. This was observed at a seasonal scale and reported in Jalón-Rojas et al. (2018).

We hypothesize that changes in tides triggered by these different pressures and changes in river discharge may have fed back into the sedimentary (and geomorphological) changes. The Gironde-Garonne system provides therefore an excellent study case to gain a better understanding of the related evolution of hydrology, morphology, hydrodynamics, and sediment dynamics under the effects of natural external forcing and human activity.

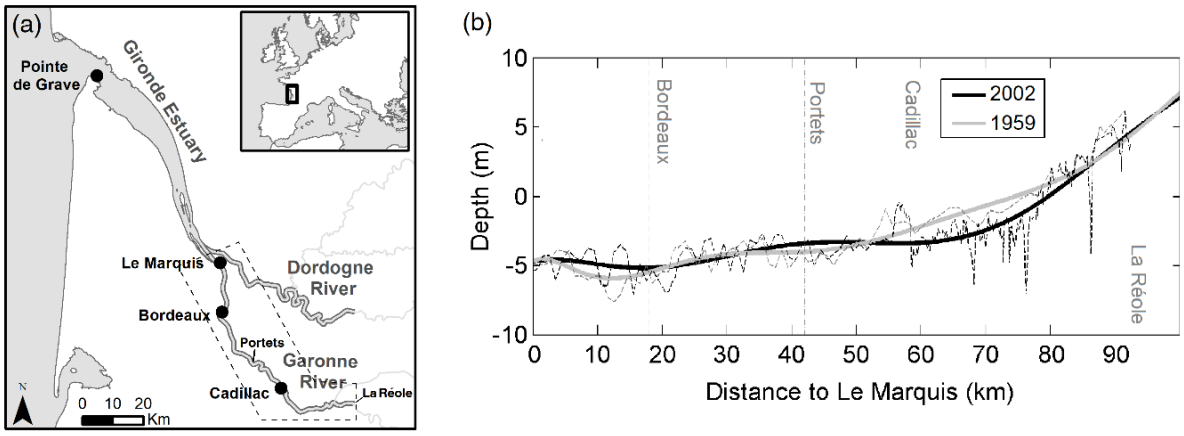

Figure 1. (**a**) Map of the Gironde-Garonne fluvio-estuarine system. Black circles indicate the location of the tidal gauges. Dotted lines delimit the model domain. (**b**) Width-averaged depth of the GTR (dotted lines) for the years 1959 (grey) and 2002 (black), and their 10th-degree polynomial fits (thick lines).

2. Methods

2.1. Study site

The Garonne Tidal River (GTR) is located on the French Atlantic coast (Fig. 1.a). It runs from its confluence with the Dordogne River, with which it forms the Gironde Estuary, to the limit of tidal influence at La Réole, 95 km upstream (Fig. 1.a). At the confluence of the rivers, the GTR is over 880 m wide and has an average depth of 5 m. At the end of tidal influence, the tidal river converges to a width of about 100 m, and the depth depends on river discharge. Nowadays, the Garonne river discharge varies from 50 to 4720 $m^3 s^{-1}$ (Banque Hydro, www.hydro.eaufrance.fr), and the typical discharge during dry periods from 100 to 400 $m^3 s^{-1}$ (Jalón-Rojas et al., 2018).

The Gironde-Garonne system is macrotidal, hypersynchronous, and flood dominant (Allen et al., 1980). The tidal range at the Gironde's mouth varies between 2.5 m and 5 m on mean neap/spring tides (Bonneton et al., 2015). Both tidal range and current velocities increase from the Gironde's mouth to around Cadillac (Fig. 1.b) due to the convergent width, and rapidly decrease in the narrow upstream sections, as a result of frictional dissipation (Ross et al., 2016; Jalón-Rojas et al., 2018). The symmetric tidal wave at the mouth becomes increasingly distorted up-estuary (shorter and stronger flood currents) due to the increasing friction (Ross et al., 2017; Jalón-Rojas et al., 2018).

The tidal pumping generated from tidal asymmetry is the main mechanism leading to landward transport, (Allen et al.,, 1980; van Maanen and Sottolichio, 2018). Combined with seaward transport resulting from river discharge, it controls the postion, persistence and concentration of a pronounced TMZ (Jalón-Rojas et al., 2015). Therefore, river discharge is the primary environmental forcing influencing the turbidity variabilityin the GTR (Jalón-Rojas et al., 2017). The TMZ occurs in the GTR at river flows lower than 200–300 m^3/s, with sediment concentration reaching values between 1 g/L and 5-5.5 g/L in surface waters (Jalón-Rojas et al.,

2015; 2017). At higher river discharge, the TMZ is progressively flushed downstream to the lower Gironde estuary.

2.2 Model description

In this study, we apply the modelling framework iFlow (v2.5, Dijkstra et al. 2017; Brouwer et al., 2018). iFlow is an idealized width-averaged 2DV model suited for the systematic analysis of flow and sediment transport in tide-dominated single-branch estuaries and rivers. It uses scaling and perturbation methods to provide an asymptotic approximation to the continuity, non-linear momentum, suspended-sediment, and trapping equations. The perturbation approach is based on the assumptions that: (1) the amplitude of the M2 tide is small compared to the mean water depth ($A_{M2}/H<<1$); and (2) estuarine geometry can be parametrized by smoothed width and depth profiles (Fig. 2.a). This approach allows us to analyze the effect of individual physical processes on the water motion and sediment transport, and the sensitivity of these processes to model parameters. Furthermore, the system is assumed to be in morphologic equilibrium, i.e., there is no bed evolution over a tidal cycle. The assumption of morphological equilibrium is valid when the fine sediments are redistributed on a time scale much shorter than the scale on which the forcings change significantly (Chernetsky et al., 2010).

The implementation of iFlow to the GTR incorporates three main novelties with respect to previous applications. Firstly, the model domain is extended beyond the limit of tidal influence by a mild-slope river region, such that the tidal signal is completely dissipated (Fig. 2). Secondly, the bottom level (z=-H) of the GTR lies above mean sea level (z=0, Fig. 2.a) in its upper reaches, so the water level depends on river flow. This behavior was reproduced by using the backwater curve $R(x)$ corresponding to the river discharge Q (Fig. 2.a) as the reference surface level. The surface level relative to z=0 is thus denoted by R+ζ, where R is the river-induced mean surface level and ζ denotes the surface elevation (Fig 2.a; more details in Dijkstra et al. 2017). Finally, the partial slip parameter defining bottom roughness (form drag + skin friction) $s_{f,0}$ in the hydrodynamic model is allowed to vary spatially (Fig 2.c, details in Section 2.3). The skin friction determining the bed shear stress for sediment erosion is kept spatially constant to simulate the erosion of muddy sediments.

The model is forced by an M_2 tide and an M_4 tide at the mouth (x=0, Fig. 2.a) and a constant river discharge at the landward boundary (x=L, Fig. 2.a). The eddy viscosity A_v is expressed as $A_v = \frac{1}{2} s_{f,0}(H + R)$, which was obtained by parameterizing the results of a large number of κ-ε model experiments (Dijkstra et al. 2017). As the salinity front is mostly downstream of the study region (van Maanen and Sottolichio, 2018), salinity is not considered. Sediments are represented by one fine sediment fraction with constant settling velocity (w_s) representing the settling velocity of typical flocs. Readers should refer to Dijkstra et al. (2017) for a detailed description of the model.

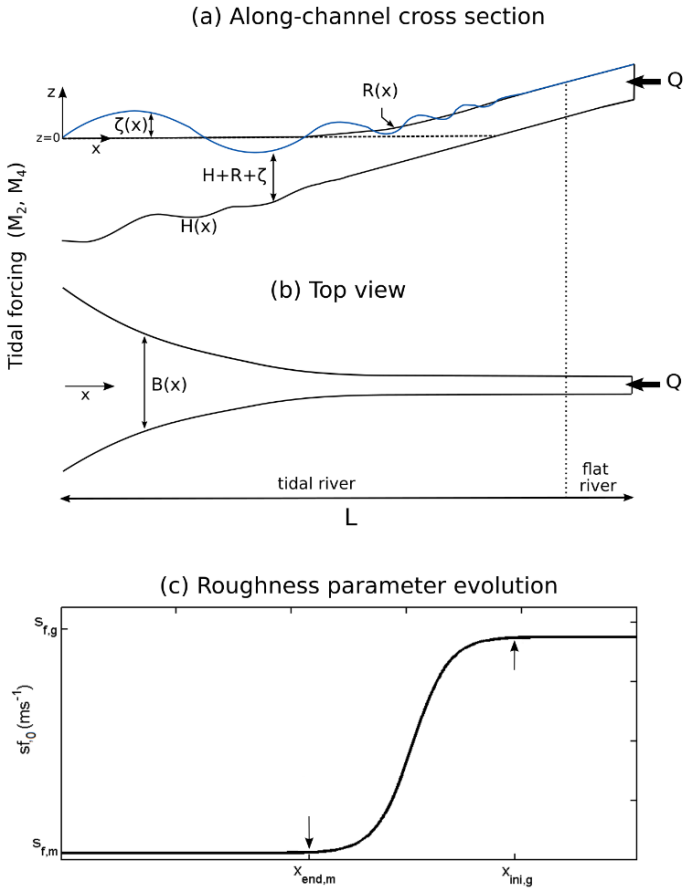

Figure 2. (**a-b**) Geometry of the tidal river in the idealized model. (**c**) Evolution of the partial slip parameter $s_{f,0}$ over the longitudinal axis x, modelled by a hyperbolic-tangent function.

2.3 Model settings

iFlow was set-up on the GTR along a longitudinal domain of 100 km, from Le Marquis (x=0, close to the confluence of the Garonne and Dordogne Rivers, Fig. 1) to 8.5 km upstream of the limit of the tidal influence (La Réole, x = 91.5 km, Fig. 1). This domain was extended a further 50 km (L=150 km) by a mildly-sloping fluvial region to ensure the complete dissipation of tidal waves, but only the first 100 km were analysed. Bathymetry data, available for the years 1959 and 2002, were provided by the Bordeaux Harbour Authority. The schematic depths $H(x)$ were determined by smoothing the width-averaged bed levels (Fig. 1.b). The strongly converging width profile has been practically constant over the last few decades, and is approximated by an exponential function (see details in the Supplementary Material).

The Bordeaux Harbour Authority also provided continuous water-level records from their stations at Pointe de Grave, Le Marquis, Bordeaux, and Cadillac (Fig. 1; dataset available at SEANOE repository for the years 1953, 1971, 1982, 1994, 2005, and 2014; Fort et al., 2018; Jalón-Rojas et al., 2018). Water-level data at Le Marquis (Fig. 1, x=0) were used to force the model. The amplitudes A_{M2}, A_{M4} and phases Φ_{M2}, Φ_{M4} of the M_2 and M_4 tides at Le Marquis depend on the morphology of the lower Gironde Estuary, on river discharge, and on the tidal

amplitude at the open ocean, which all vary over time (Jalón-Rojas et al., 2018). Each model scenario is therefore forced by a different A_{M2}, A_{M4}, Φ_{M2} and Φ_{M4} depending on the year of simulation Y (to account for changes in the lower Gironde morphology), the river discharge Q, and the tidal range at Pointe de Grave TR_{PDG}, close to the open ocean. For each model scenario (Y, Q, TR_{PDG}), we calculated the time series of each tidal forcing parameter by applying the Complex Demodulation Method to water-level data at Le Marquis (results in Jalón-Rojas et al., 2018). Then, we calculated the mean value of each parameter in year Y, during periods with river discharge $Q \pm 25$ m^3/s and tidal range $TR_{PDG} \pm 0.25$. These values are given for all scenarios in Supplementary Material. This same procedure was applied to calculate the tidal properties at Bordeaux and Cadillac in order to calibrate and validate the model. The calculated values of A_{M2} and A_{M4} at the three stations are shown in Figure 4 for a low river discharge

The partial slip parameter $s_{f,0}$ (form drag + skin friction) of the hydrodynamic model varies along the GTR bed and over time, i.e. over the scenarios, following the different soil types of the bed : (a) muddy and sandy deposits from Le Marquis (x=0 km) up to $x_{end,m}$, a section defined by the TMZ position and intensity – this section moves upstream during and after occurrence of the TMZ, and downstream during river floods (Jalón-Rojas et al., 2015; 2018); (b) sandy deposits from $x_{end,m}$ to the beginning of gravel soils $x_{ini,g}$; and (c) gravel soils from $x_{ini,g}$ to the end of the domain. This rugosity variability was approximated by the hyperbolic tangent defined in Fig. 2.c, where $s_{f,m}$ and $s_{f,g}$ are the partial slip parameters for muddy and gravel beds, respectively, $x_{end,m}$ defines the upper limit of the muddy bed, and $x_{ini,g}$ is the downstream limit of the gravel bed . $s_{f,m}$ is also the skin friction of the sediment model.The determination of these four parameters, together with the settling velocity w_s and the suspended-sediment concentration at the lower boundary $c_{x=0}$, is described in Section 2.4.

2.4. Historic scenarios and calibration methods

iFlow was applied to a total of 20 scenarios, representing 4 years/morphologies, 5 river discharges, and 1 tidal range at the open sea (Table 1), taking into account the availability of tidal and bathymetry data. The four selected morphological years were 1953, 1971, 1994, and 2014, for each of which five river discharges were simulated: 125 m^3/s; 200 m^3/s; 375 m^3/s; 675 m^3/s; and 900 m^3/s. The main reason for selecting these years was the availability of water-level time series at Le Marquis during these periods. As explained in Section 2.3, the bathymetry of the lower Gironde for each year impacts the hydrodynamics and therefore the forcing tidal inputs at the model mouth (Le Marquis station). A mean tidal range of spring tides at the open sea (Pointe de Grave), T_{PDG}=3.75 m, was selected based on two criteria: (1) the higher availability of water-level observations during spring tides for all the discharge situations; and (2) the prospect of reproducing conditions such as the uppermost limit of the TMZ. The GTR depth profile of 1959 was used for the years 1953 and 1971; in the second case, it was deepened by 1.5 m between x = 56 km and x = 78 km in order to simulate the gravel extraction (Castaing et al., 2006). The GTR depth profile of 2002 was used for the years 1994 and 2005. Even though the GTR bathymetry data do not correspond exactly to the investigated years, the individual calibration of each scenario allows accurate reproduction of the hydrodynamics.

Table 1. Characteristics of the 20 simulated scenarios.

Historic scenarios		
Year (Y)	**River flow (Q, m^3/s)**	**Tidal range at the open sea (TR_{PDG} ,m)**
1953	125	3.75
	225	
1971	375	
1994	675	
2014	900	

The hydrodynamic model was calibrated to observations of A_{M2}, A_{M4}, Φ_{M2} and Φ_{M4} at Bordeaux and Cadillac (observed values calculated as explained in Section 2.3) and river-flow set-up along the GTR. In particular, we determined the values for the four variables $s_{f,m}$, $s_{f,g}$, $x_{end,m}$ and $x_{ini,g}$ defining the bottom stress parameter $s_{f,0}$ (Fig. 2.c). All the scenarios were characterized by the same stress parameters of gravel and muddy soils ($s_{f,g}$, $s_{f,m}$). The downstream limit of gravel soils $x_{ini,g}$ is also considered invariable over the last decades according to the literature (Castaing et al., 2006; ARTELIA, 2015). The upper limit of muddy beds $x_{end,m}$ was calibrated for each individual scenario to give an accurate reproduction of the hydrodynamics. This parameter was found from a least-squares fit between observed and modelled water levels at Bordeaux and Cadillac using the cost function introduced by Jones and Davies (1996). A detailed explanation of the calibration processes, together with the resulting values is provided in Section 3.1.

Values for the sediment-model parameters, settling velocity w_s and the surface suspended-sediment concentration (c) at the lower boundary ($c_{x=0}$) were determined by calibrating sediment concentrations from recent scenarios (2014) to surface concentration data available for Bordeaux (x = 18 km) and Portets (x = 43 km) from the automatic continuous monitoring network MAGEST (Etcheber et al., 2014; Jalón-Rojas et al., 2015). Apart from the direct comparison of observed and modelled c, we verified the accurate representation of the concentration level and variability at these stations using Singular Spectrum Analysis (SSA). SSA is a principal-components analysis in the time domain that decomposes time series into a sum of reconstructed components (RCs) characterized by an almost constant frequency, and calculates the relative contribution of each RC to the total variance (details in Vautard et al., 1992 and Jalón-Rojas et al., 2016a). This method identifies the variability time scales (RCs) of a time series and their relative importance. Therefore, the comparison of the observed and modelled RCs of c and their contribution to the total variance allows us to discuss how accurately the model reproduces the observed variability time scales of suspended sediment concentrations.

This calibration for the year 2014 aims to demonstrate that the model reproduces the correct patterns and magnitude of c. However, due to the lack of historical data of sediment

concentrations, $c_{x=0}$ cannot be determined for the other years. Therefore, we will focus on the changes of the spatial patterns of c over the decades, and not the magnitude. To do this, the concentration will be scaled with the seaward concentration (i.e. $c/c_{x=0} = 1$ at x=0, for all the scenarios) which provides the spatial pattern of concentration without claiming anything about the magnitude. This approach helps to highlight the changes induced by morphological and hydrological alterations since all the other conditions (i.e. changes in the sediment properties, boundary conditions and therefore sediment budget) are ignored.

3. Model calibration and results

3.1. Calibration and validation

The hydrodynamic model was calibrated to observations of water motion and river-flow set-up along the GTR following the methods described in Section 2.4. The four calibration variables $s_{f,m}$, $s_{f,g}$, $x_{end,m}$,and $x_{ini,g}$ defining the bottom stress parameter $s_{f,0}$ (Fig. 2.c), were determined as follows:

– $x_{ini,g}$: the downstream limit of gravel soils in Eq. (2) was set to 80 km, so that the stress parameter of gravel soils $s_{f,g}$ was quasi-constant upstream from Langon (x = 67 km), the real downstream limit of gravels and pebbles according to literature (Castaing et al., 2006; ARTELIA, 2015).

– $s_{f,g}$: the stress parameter of gravel soils was set using two criteria: (1) the modelled upstream limit of tidal influence should be around La Réole (x = 91.5 km, Fig. 1), even with low river discharge; and (2) it must provide a river-flow set-up close to observations. The first criterion was met by $s_{f,g} > 0.05$. The set-up induced by a river discharge of 125 m^3/s during the year 2014 was modelled for values of $s_{f,g}$ between 0.05 and 0.125, and compared with the observed set-up in similar conditions during 2002 (Fig. 3, Castaing et al., 2006). As a result of this comparison, $s_{f,g}$ was set to 0.075.

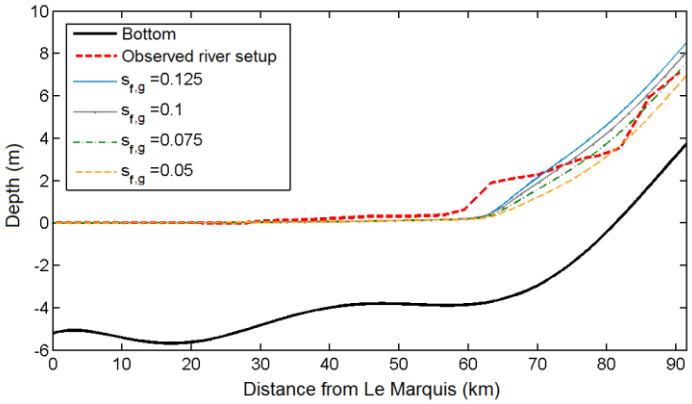

Figure 3. Comparison of observed and modelled river-flow set-ups for different values of $s_{f,g}$.

– $s_{f,m}$: the stress parameter for muddy beds was determined from the model scenario of low river discharge (125 m^3/s) during 1994. For this scenario, muddy sediments from the TMZ were estimated to reach the Cadillac station (Castaing et al., 2006; Chanson et al., 2011). For this scenario, the upper limit of muddy deposits was $x_{end,m}$ = 42 km in Eq. (2), so that the stress parameter of muddy soils $s_{f,g}$ was quasi-constant up to Cadillac (x = 56 km). Water motion was simulated using values of $s_{f,g}$ between 0.001 and 0.01. Observed and modelled water levels were compared using Eq. (3), resulting in an optimal value of the stress parameter for muddy beds of $s_{f,g}$=0.022.

– $x_{end,m}$: the upper limit of muddy beds was determined for each individual scenario using Jones and Davies´s cost function. Figure 4.a-b shows the comparison between the observed and modelled amplitudes and phases of the frequency components of water level for all the years and low river discharge conditions. In general, there was a good agreement with the M2 water level and phase, the M4 water level in the lower GTR, and the M4 phase (see phases comparison in Supplementary Material, Figure S1). However, there was an overestimation of the M4 water level in the upper GTR, probably related to the simplification of bathymetry and bottom roughness. The amplitudes of the M_2 and M_4 current velocities were further validated for the 2014 scenario with low river discharge (Fig. 4.c-d). This calibration ensured a reasonably accurate reproduction of the hydrodynamics of each scenario. The result of the calibration shows that $x_{end,m}$ increased over time, which corresponds to gravel extraction and the shift upstream of the TMZ (values given in Supplementary Material).

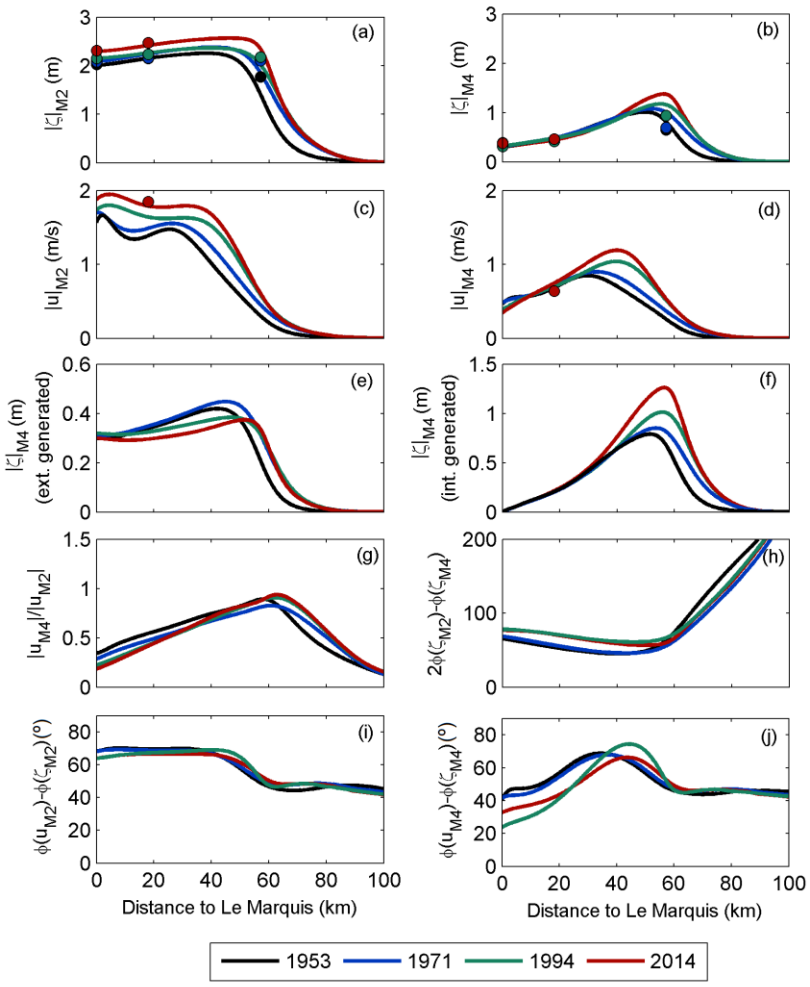

Figure 4. Multi-decadal evolution of hydrodynamic parameters: water level amplitude of the M_2 (**a**) and M_4 (**b**) components; current velocity amplitude of the M_2 (**c**) and M_4 (**d**) components; water level amplitude of the (**e**) externally forced M_4 and the (**f**) internally generated M_4; horizontal tidal asymmetry distorsion (**g**) and vertical tidal asymmetry direction (**h**); phase differences between tidal currents and tidal height for M_2 (**i**) and M_4 (**j**) components. These results correspond to scenarios of spring tide (tidal range of 3.75 m at the estuary mouth) and low river discharge (125 m^3/s). Dots represent observations at (downstream to upstream) Le Marquis, Bordeaux and Cadillac stations.

The settling velocity w_s and the surface suspended-sediment concentration at the lower boundary $c_{x=0}$ were determined by calibrating the modelled surface concentration against observations from MAGEST (Section 2.4).. We first determined w_s using a low river discharge (125 m^3/s) and spring tide, for which the TMZ spreads from Le Marquis to Cadillac, with the highest concentrations between Bordeaux and Cadillac (Jalón-Rojas et al., 2015). The value of the settling velocity w_s is known for the lower Gironde Estuary, and ranges from 0.1 mm/s (floc size < 40 µm) to 3 mm/s (floc size > 640 µm) according to Manning et al. (2004). In the GTR, particle sizes are small, except for some microflocs (Gibbs et al., 1989), so the settling velocity is

expected to be much lower than 2 mm/s. The longitudinal distribution of tidal-averaged surface concentration was calculated for values of w_s between 0.1 mm/s and 2 mm/s and values of $c_{x=0}$ between 3 and 5 g/L (we expected a value similar to the one observed at Bordeaux station): the values that best reproduced the TMZ position were selected. Figure 5.a shows the results for three values of w_s and the selected value of $c_{x=0}$, 4.15 g/L, which provides the best agreement with the observations in the lower GTR regardless of the value of w_s. The value w_s = 0.7 mm/s provided the best model reproduction of the observed location of the TMZ during low river discharge (Fig. 5.a); the TMZ was flushed too far downstream for $w_s \leq 0.5$ mm/s, and was concentrated over a very short length for $w_s \geq 1$ mm/s. The optimal concentration at the entrance $c_{x=0}$ was determined for the rest of the river flow scenarios using w_s=0.7 to demonstrate that the model is able to reproduce the concentration and TMZ patterns in 2014. Fig 5.b shows a comparison with observed concentration for a river discharge of 600 m^3/s. According to MAGEST data, discharges above 610 m3/s ensure the complete expulsion of the TMZ from Bordeaux (Jalón-Rojas et al., 2015), which was reproduced by the model satisfactorily. Due to the lack of historical data, the optimal concentration at the entrance could not be derived from data for the other years. Therefore, only the ratio of the concentration $c/c_{x=0}$ is shown for the other years (i.e. $c/c_{x=0} = 1$ at x=0, for all the historical scenarios), allowing us to evaluate the evolution of spatial trends over the decades, as explained in Section 2.4.

The model was further validated by comparing the observed and modelled time series of concentration at Bordeaux during low river discharge, as well as their time scales of variability using the SSA decomposition (Figure 5.c-h, method described in Section 2.4).. The model is able to reproduce both the level (Fig. 5.c) and variability (Fig.5.d-h) in the concentration. The four components representing the main frequencies of variability (M_2 and M_4 frequencies) were identified and accurately reproduced by the model. The only difference was that the total contribution of the four components to the total variance was higher (32% overestimated, Fig.5.h) for the model results; the model was only forced with M_2 and M_4 tides, and was not able to reproduce SSC variability at higher frequencies. The model therefore reproduced the observations with reasonable accuracy, considering all its simplifications.

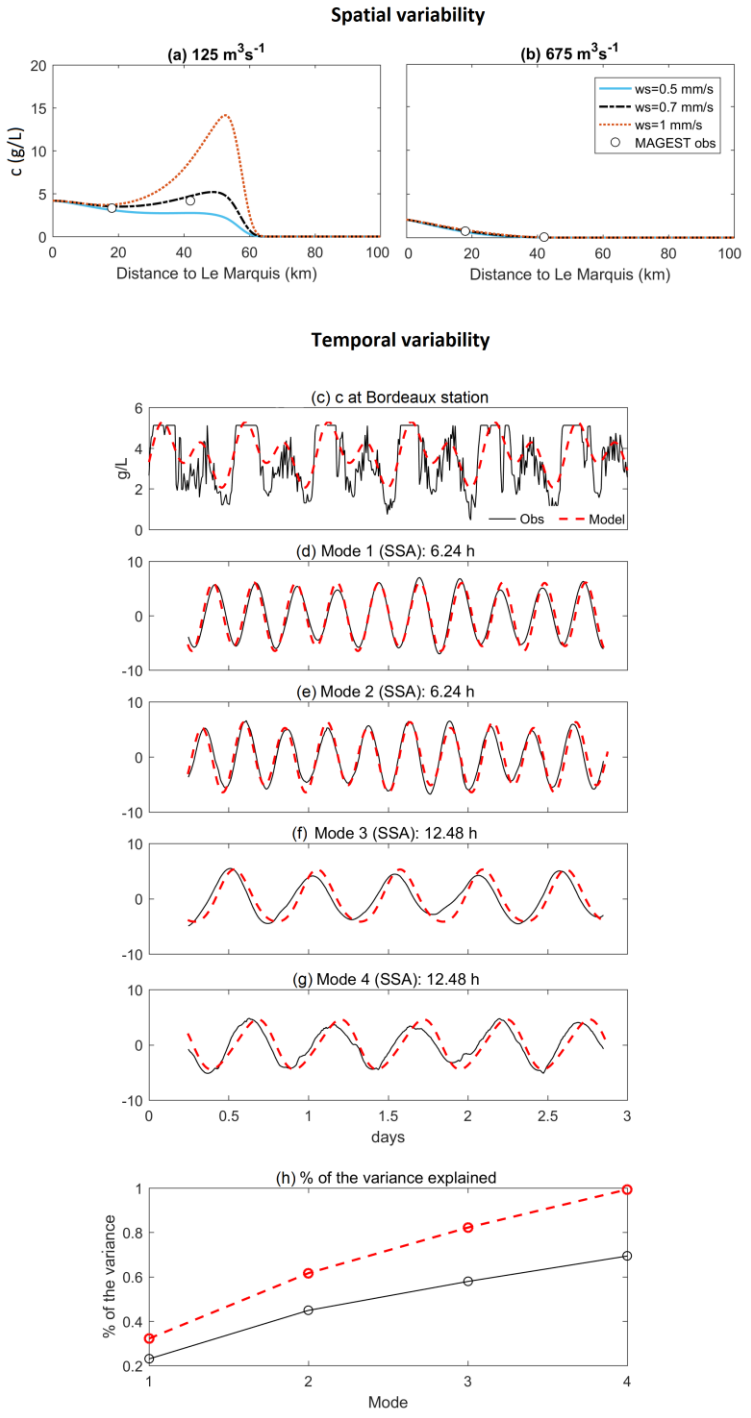

Figure 5. Spatial and temporal variability in surface suspended-sediment concentration in morphodynamic equilibrium during 2014. Tidal-averaged concentration along the GTR for three settling velocities w_s (0.5 mm/s, 0.7 mm/s, and 1 mm/s) and two river discharges: (**a**) 125 m^3/s and (**b**) 625 m^3/s. Observed and modelled time series of (**c**) concentration at Bordeaux and (**d-h**) singular spectrum analysis (SSA) decomposition. Each component is shown with its frequency

of variability (6.24 h or 12.48 h). (**f**) Cumulative contribution to the total variance (%) of each observed and modelled component .

3.2. Multi-decadal evolution of hydrodynamics

We first evaluated the multi-decadal evolution of the hydrodynamics in the GTR by comparing the amplitudes of water level and currents, tidal asymmetry parameters, and the phase lag between currents and water level for the various years. The M_4 water level was also decomposed into external (propagation upstream from the Gironde) and internal (generated inside the GTR by non-linear effects) to distinguish between the impact of morphology in the Gironde and GTR on this overtide. This decomposition can be done due to the linearity of the equations system, which allows for a separate treatment of each forcing term (Dijkstra et al., 2017). Figure 4 illustrates this comparison for similar external forcings (low river discharge and spring tides at the open ocean). The water level and velocity amplitude of the M_2 component increased gradually over the years along the whole GTR (Fig. 4.a and 4.c). For example, it increased by 0.33 m at Portets (x =43 km) between 1953 and 2014. The water level and velocity amplitudes of the M_4 component also increased gradually over the period, but from x = 40 km and x = 25 km, respectively (Fig. 4.b and 4.d). Consequently, the horizontal tidal asymmetry distortion increased over the same period at the upper reaches (from x= 40 km, Fig. 4.g). The relative phase of the vertical tide became closer to the maximum flood dominant conditions (90º) between 1971 and 1994 (Fig. 4.h). These trends were also found in the scenarios with higher river discharges, except that the tides were slightly more damped. Therefore, morphological changes over the decades led to an increase of both water level, currents and tidal asymmetry in the GTR. This trend has already been reported by Jalón-Rojas et al. (2018) at the three tidal gauges (Le Marquis, Bordeaux, and Cadillac) for the water level height and asymmetry, but these simulations allow us to generalize this outcome along the longitudinal axis and confirm the increase of the velocity components. For instance, the section of maximum amplification of tides (or the start of damping) shifted upstream by 12 km over these six decades. Similarly, the limit of tidal propagation also moved upstream by 4–6 km. The increase of the M4 tidal amplitude was mainly due to the internal generation of this component in the GTR (Fig. 4.e-f). Furthermore, the phase differences between horizontal and vertical tides remained between approximately 40° and 70° for M_2, showing a more standing character over the first 45 km of the GTR and no variations between the different years. The M4 amplitude increased over the first 30 (1953-1971) – 45 (1994-2014) km, which indicates a more standing wave character, a lower tidal damping and an increased celerity. The peak of this phase difference increased and moved upstream for the years 1994 and 2014, although values were lower for these two years in the lower GTR.

3.3. Multi-decadal evolution of suspended-sediment dynamics

3.3.1 Impact of hydrological changes on suspended-sediment concentration

The impact of river discharge on concentration was first analysed for the year 2014, for which $c_{x=0}$ could be calibrated. Figure 6 shows the tidally averaged concentration at the surface for the various river discharges. For a better evaluation of the evolution of the TMZ, and particularly its upstream limit, the right panels highlight the concentration higher than 1 g/L, the threshold value defining the TMZ in the Gironde Garonne system (Allen et al., 1980; Jalón-

Rojas et al., 2015). For low river discharge conditions, a strong TMZ extended over the first 61 km (125 m^3/s) and 51 km (200 m^3/s) from the confluence. The maximum concentrations were much large (up to 6 g/L) and located more upstream (from x=35 km) with a discharge of 125 m3/s than with a discharge of 200 m^3/s. Concentrations decreased below 3g/L with a river discharge of 375 m3/s, although the TMZ was still present over the first 38 km. The complete expulsion of the TMZ from the GTR required discharges greater than 900 m^3/s, although from 675 m3/s, a low concentrated TMZ was only present around Le Marquis (x=0).

To analyse the impact of changes in hydrology over the decades, Figure 7 compares the tidally average $c/c_{x=0}$ at the surface for 1953 and 2014 for all river discharges. From Figure 7, it is apparent that a decreasing river discharge moved the TMZ upstream for both years, but that the displacements were different between these two years. In general, the maximum relative concentration $c/c_{x=0}$ was higher and reached further upstream during 2014 for the same river discharge. For example, while the TMZ was still present over the first 40 km with a discharge of 375m^3/s in 2014 (Fig. 6.b), it was practically expulsed in 1953 for the same discharge (Fig. 7.a). These differences are a consequence of morphological changes as all the other parameters are the same. Therefore, the evaluation of the impact of multidecadal hydrological changes on the TMZ needs to consider the concomitant impact of morphological changes, and will be analysed in Section 3.3.2.

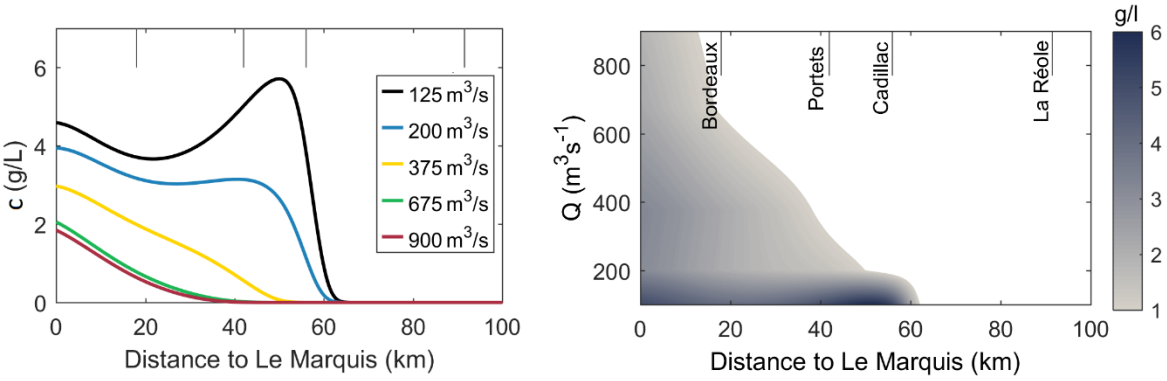

Figure 6. Evolution of tidally-averaged concentration c at the surface of the GTR with river discharge for the year 2014. Right panels show the interpolation of data presented in left panels, highlighting values higher than 1g/L (TMZ ocurrence).

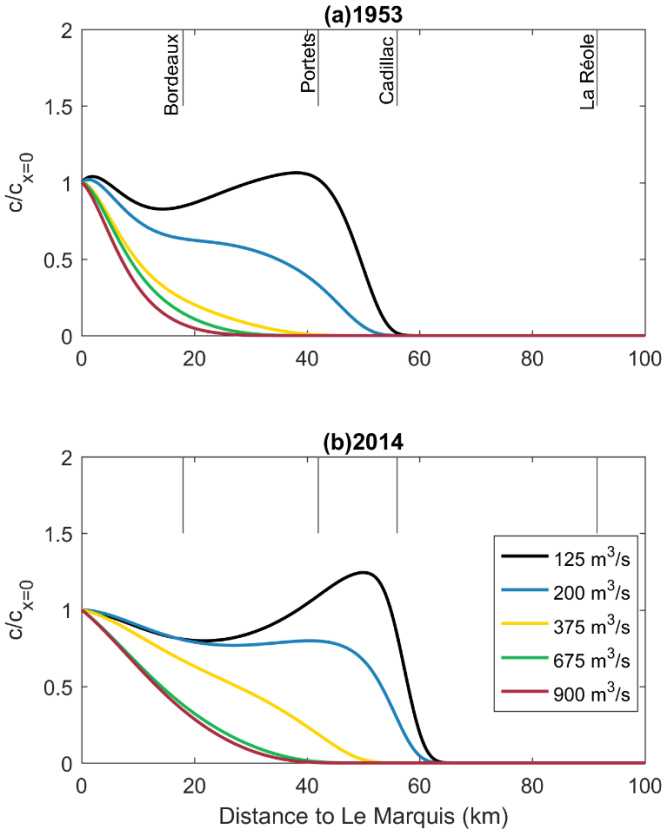

Figure 7. Evolution of tidally averaged $c/c_{x=0}$ at the surface of the GTR with river discharge for the years (**a**) 1953 and (**b**) 2014.

3.3.2 Impact of multidecadal morphological and hydrological changes on suspended sediment concentration

The multi-decadal changes of the hydrodynamics in the GTR due to morphological and hydrological changes (Section 3.2) has implications for the sediment transport. Figure 8 illustrates the multi-decadal evolution of the tidally averaged $c/c_{x=0}$ at surface waters of the GTR for all river discharges considered. The TMZ threshold (1 g/L / $c_{x=0}$) of 2014 was selected in the right panels to highlight the TMZ upstream limit and discuss the changes in patterns qualitatively. In low river discharge conditions (125 m^3/s, Fig. 7.a), a well-defined TMZ extending from Le Marquis to several tens of kilometres upstream was formed in all years. However, the core (region of maximum concentrations) and the upper limit (upper reach with c= 1 g/L, i.e. $c/c_{x=0} = 1/c_{x=0}$, Jalón-Rojas et al., 2015) of the TMZ has progressively moved upstream according to the simulations. In 1953, the most turbid surface waters were located between x = 25 km and x = 40 km, downstream of Portets. From 1994, they were located between x = 40 km and x = 52–56 km, between Portets and Cadillac. In conclusion, between 1953 and 2014, the upper limit of the TMZ shifted upstream by 7.5 km. The multidecadal trend of $c/c_{x=0}$ is quite similar for 200 m^3/s (Fig. 8.b). Considering 2014, the upper limit of the TMZ progressively

shifted upstream by 15 km since 1953, from x=43 km to x=58 km. For these low river discharges, the largest adjustment took place between 1971 and 1994. The level of concentration significantly increased between these years and the upper limit of the TMZ moved 5.5 km and 8 km upstream for river discharges of 125 m3/s and 200 m3/s. With a river discharge of 375 m^3/s (Fig 8.c), almost the entire tidal river had concentrations lower than the TMZ threshold in 1953. A diluted TMZ extended more and more upstream over the decades. For this river discharge, the most drastic change was observed between 1994 and 2014 ; the upper limit of the TMZ moved 14 km upstream (from x = 23.5 km to x = 37.5 km), while the displacement between 1953 and 2014 was 24 km. With a river discharge of 675 and 900 m^3/s (Fig. 8.d-e), the TMZ is practically expulsed from the GTR for all years, in particular for 1953. Between 1953 and 2014, the upper limit of the TMZ was displaced by 5-6.5 km. In conclusion, the multidecadal morphological changes resulted in a gradual increase of the relative concentration $c/c_{x=0}$ and the upper limit of the TMZ over time.

These results also make it possible to compare, within the limits of the model assumptions, the relative or accumulated effects of the morphological and hydrological changes on the TMZ. For example, in the 2014 scenario, the TMZ displacement induced by a decrease in mean summer river discharge from 200 m^3/s (typical summer discharge in the 1950s) to 125 m^3/s (close to the typical summer discharge in the 2010s) would be around 4 km (Fig 8.a-b). This displacement is considerably lower than the displacement induced by morphological changes between 1953 and 2014 (of around 10 km and 15 km for 125 m^3/s and 200 m3/s, respectively). The cumulative displacement caused by both impacts (from 200 m^3/s in 1953 to 140 m^3/s in 2014) would be around 19 km (Fig. 8).

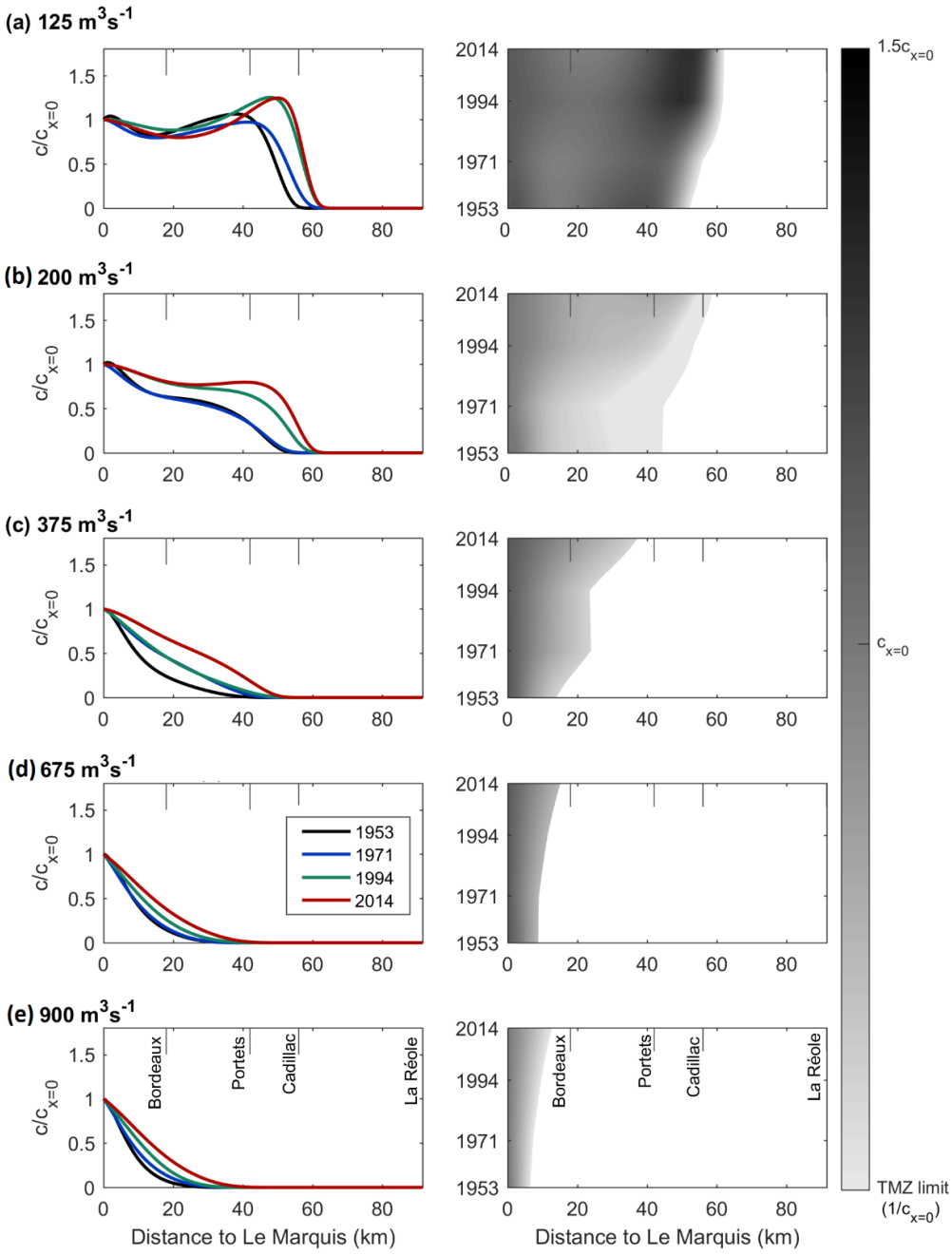

Figure 8. Multi-decadal evolution of tidally averaged $c/c_{x=0}$ at the surface of the GTR for five levels of river discharge: (**a**) 125 m^3/s; (**b**) 200 m^3/s; (**c**) 375 m^3/s; (**d**) 675 m^3/s and (**e**) 900 m^3/s. Right panels show the interpolation of data presented in left panels over time.

4. Discussion

4.1. Multidecadal evolution of sediment trapping

To understand better the multi-decadal evolution of upstream sediment trapping, we evaluated the evolution of the transport capacity (the sediment transport that occurs when there is an abundance of sediment on the bed everywhere in the estuary) and of the different physical mechanisms contributing to it (Dijkstra et al., 2019c):

- The *river* contribution is the transport capacity due to the tidal asymmetry caused by the tide-river interaction and the river-induced flushing of tidally resuspended sediment.
- The *river-river* contribution is independent of the tide and represents the river-induced flushing of sediment resuspended by the river.
- The *external M_4 tide* contribution is due to tidal asymmetry caused by the M_2 tide and M_4 tidal forcings (i.e., the velocities and concentrations resulting from the prescribed M_4 sea surface elevation at the entrance).
- The horizontal *sediment advection* or *spatial settling lag* contribution is due to spatial settling lag effects (see, e.g., De Swart & Zimmerman, 2009). It is also defined as the tide-averaged effect of advection of sediment (Friedrichs, 2012).
- The *tidal return flow* contribution is due to Stokes drift (sediment import) and the corresponding return flow (sediment export). The return flow velocity also has a M4 contribution, which may cause import or export of sediment, depending on the phase-lag with the M2 tide.
- The *no flux* contribution represents the asymmetric concentration of sediments during ebb and flood due to the distribution of resuspended sediments over different water column heigths.
- The *velocity-depth asymmetry* contribution represents the effect that the velocity profile differs between ebb and flood due to different water levels.

Figure 9 shows the contribution of these mechanisms to the total transport capacity of suspended sediment (T_{total}) in all years for two values of the river discharge: 125 m^3/s and 375 m^3/s. Positive and negative values denote upstream and downstream transport capacity, respectively; the zero-crossing from positive to negative corresponds to convergence zones and the approximate location of the TMZ. The river and river-river contributions were the main components inducing differences between the two river discharge experiments. These components led to sediment export together with the no flux and the velocity-depth asymmetry contribution, these last two to a smaller extent. In both cases, the river contribution increased over the decades downstream of x = 60 km. In the low river discharge scenario (Fig. 9.I), this increase of the river-induced export was balanced by an increase of the components leading to sediment import (external M4 tide, sediment advection and tidal return). For high river discharge scenarios (e.g., Fig. 9.II), the river contribution was a dominant mechanism influencing the total transport capacity. As a consequence, the total transport was directed downstream for all scenarios with discharge larger than 375 m^3/s, whereas two convergence points indicating the TMZ formation appeared in all the 125m^3/s scenarios. For a low river discharge (Fig. 9.I), the

multi-decadal changes in the transport capacity and the TMZ position were largely due to changes in the sediment advection contribution; its maximum value was close to the downstream boundary x = 0 in 1953 and 1971, but moved to around x = 40 km and x = 45 km in 1994 and 2014, respectively. The external M4 tide and tidal return flow components also influenced the total transport; they had a greater amplitude and decreased to zero slightly more and more upstream over the decades. These trends agree with the computed hydrodynamics (Section 3.2, Fig. 4). Even if it is difficult to explain the transport capacity components in term of the tide due to the complex non-linear interactions, it is noticiable that the components inducing upstream transport peaks (sediment advection, external M4 tide, tidal return flow) at sections characterized by maximum values of velocity currents and phase differences between vertical and horizontal tides (e.g. around x=10 km and x=45 km in 2014, see Figure 4 and Figure 9). Similarly, the increase and upstream displacement of the peaks of these components over the decades agrees with the the increase and upstream displacement of the maximum values of the M_2 and M_4 water level and velocity, the tidal asymmetry, and the phase difference of horizontal and vertical M_4 tide (Section 3.2., Figure 4). .

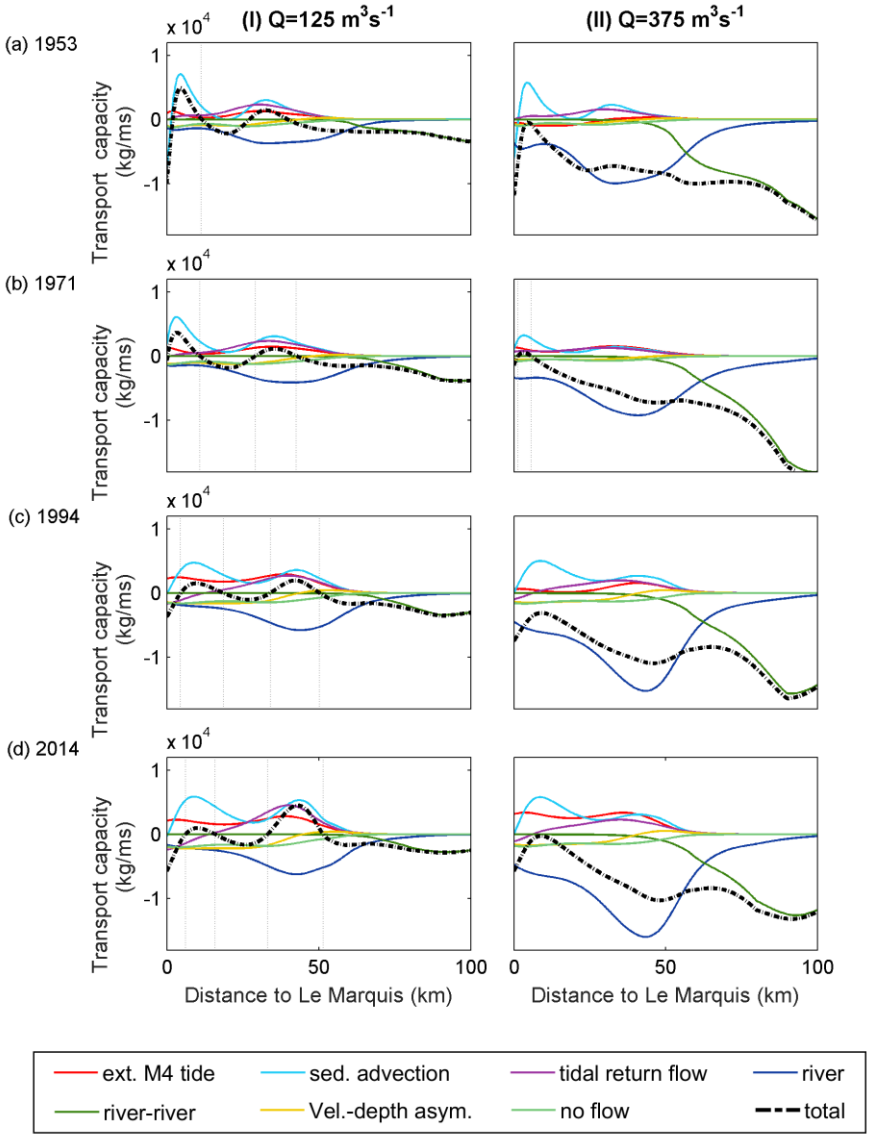

Figure 9. Contribution of the different physical mechanisms to the sediment transport capacity per meter width (and integrated over depth). Negative values indicate export, while positive values indicate import. The total net transport of all term is plotted in black dashed line.. Spring tide (tidal range of 3.75 m at the estuary mouth) and river discharges of (**I**) 125 m^3/s and (**II**) 375 m^3/s for (**a**) 1953, (**b**) 1971, (**c**) 1994, and (**d**) 2014.

4.2. Relative impact of multidecadal geomorphological changes on sediment trapping

Whereas in the previous sections we have looked at the total differences between the scenarios, we now distinguish between the relative importance of the different geomorphological impacts (climate-induced morphological changes in the lower Gironde, deepening of the upper Garonne for gravel extraction, and changes in mud roughness) on the hydro-sedimentary dynamics. For that purpose, four morphological scenarios (1953, 1971, 1994, and 2014) with a flow rate of 200 m^3/s (typical river flow during dry periods in all the decades; Jalón-Rojas et al., 2018) were selected as reference scenarios (Fig. 10.I). Twelve additional scenarios (4 years × 3 geomorphological variations) were created from the reference scenarios to analyse the different pressures separately. The three geomorphological variations were:

1. Not including the climate-induced morphological changes in the lower Gironde. This is represented by forcing the model with the same tidal amplitudes and phases at Le Marquis, namely those of 1953, for all scenarios. These results are shown in Fig. 10.II;
2. Not including morphological changes in the GTR, particularly the deepening of the upper sections. This is done by using the same morphology of the GTR, that of 1953, for all scenarios (morphology before gravel extraction). Results depicted in Fig. 10.III;
3. Not including the changes in bed roughness, particulary in the upstream shift of muddy bed. This is represented in the model by the same upper limit of the mud beds $x_{end,m}$, that of 2014, for all scenarios; see Fig. 10.IV.

We compared the multi-decadal evolution of $c/c_{x=0}$ for the four (reference+variations) geomorphological situations in order to determine the relative impact of each pressure on sediment dynamics (Fig. 11.a). The multi-decadal evolution of the main transport capacity components for the same geomorphological simulations is shown in Fig. 10.

The multi-decadal evolution of $c/c_{x=0}$ for the reference scenarios (Fig 8.b and 10.I.a) has already been described in Section 3.3. According to the simulations, the upper limit of the TMZ was displaced from x = 43 km in 1953 to x = 58 km in 2014, and the $c/c_{x=0}$ gradually increased over the decades as a consequence of the evolution of the transport mechanisms inducing sediment import. The peaks of the sediment advection transport capacity (Fig 10.I.b) have shifted upstream from x = 4 km and x= 32.5 km in 1953 to x = 9 km and x = 44.5 km in 2014, while the second peak has also increase in magnitude. The tidal return flow transport capacity (Fig 10.I.c) have experienced this same trend. In both cases, the main upstream displacement occurred between 1971 and 1994, around 8 km, while the main increase of the magnitude occurred between 1994 and 2014. The external M4 tide component (Fig. 10.I.d) has mainly increased in magnitude progressively over the decades. The seaward river transport capacity (Fig 10.I.e) also increased between 1971 and 1994 but this increase was not enough to hamper the upstream displacement of the TMZ.

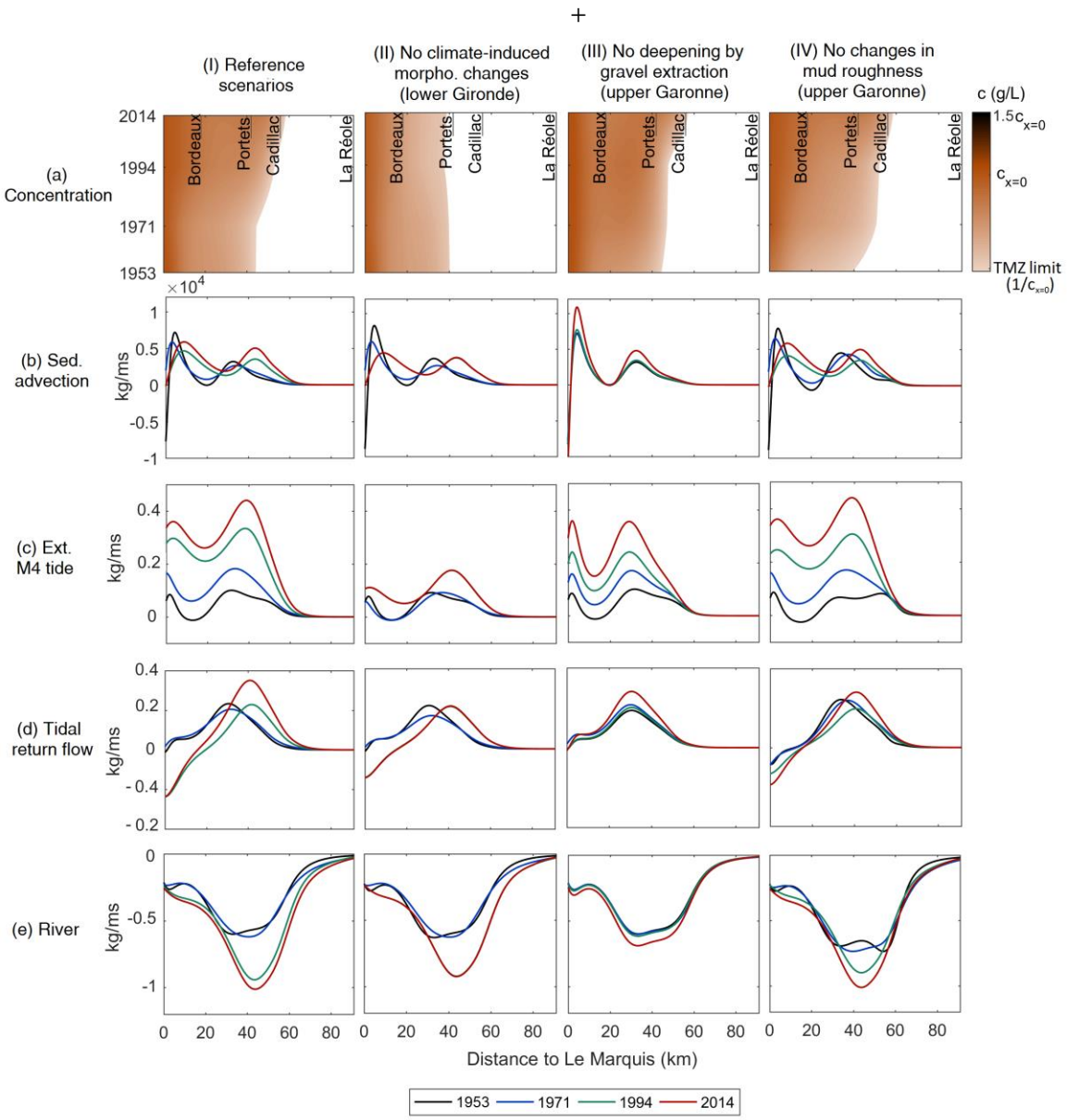

Figure 10. Multi-decadal evolution of: (**a**) tidally averaged surface concentration (g/L); (**b**) sediment advection transport capacity (kg/ms) ; (**c**) external M4 tide transport capacity (kg/ms); (**d**) tidal return flow transport capacity (kg/ms); and (**e**) river transport capacity (kg/ms), for each of the four morphological situations: (**I**) the actual morphology (reference scenarios); (**II**) not considering the climate-induced morphological changes of the lower Gironde; (**III**) not considering the deepening of the GTR; (**IV**) not considering changes in the bed roughness of the GTR. River discharge of 200 m^3/s.

When the morphology of the lower Gironde, and therefore the tidal forcing at Le Marquis, was considered invariant after 1953, the TMZ boundary and $c/c_{x=0}$ also remained

invariant over time (Fig. 10.II.a). In this scenario, the external M4 tide components barely changed over time (Fig 10.II.b), as well as the magnitude of the other components inducing upstream transport (Fig 10.b.a-c). Only the peaks of the sediment advection and tidal return flow transport capacity changed between 1971 and 1994. These results suggest that the evolution of transport capacity related to the external M4 tide caused by morphological changes in the lower Gironde was a key factor in the evolution of the sediment dynamics in the GTR.

When the bathymetry of the GTR remained constant over the decades since 1953, the upper limit of the TMZ showed a similar total shift between 1953 and 2014, compared to the reference scenario (Fig. 10.III.a). However, the TMZ displacement between 1971 and 1994 was lower in the reference. This is because the multidecadal evolution of the external M4 tidal transport capacity is similar to the reference scenario, but the upstream displacement of the sediment advection and the tidal return flow components between 1971 and 1994 did not occur (Fig. 10.III). These results show that the morphological changes in the upper GTR have a minor influence on the TMZ dynamics, and confirm that the effect of climate-induced morphological changes in the lower Gironde on the external M4 tide and the TMZ dynamics is dominant.

The last variation showed the multi-decadal evolution of the transport processes, when the upper limit of muddy deposits was considered invariant and equal to the value of 2014 (Fig. 11.IV). The evolution of c was very similar to the reference scenarios, with two differences: the upper limit of the TMZ was 7 km more upstream for 1971 and 5 km more downstream for 1953 compared to the reference scenarios (Figs. 11.I.a and 11.IV.a). For both years, the sediment advection and the tidal return transport capacity increased between Portets and Cadillac due to the lower roughness in this region, (Figs. 11.IV.b and 11.IV.d) but also to the downstream river transport capacity. In 1953, the enhanced river transport capacity is higher than the import transport components from x = 40 km and shifted the TMZ upper boundary downstream. In 1970, the TMZ arrived in this region due to the higher external M4 tidal transport capacity related to the climate-induced morphology of the lower Gironde; the combined effect of these morphological changes and the lower roughness in the upper GTR led to an upstream shift of the TMZ compared to the reference scenario. These results support the fact that, even if the geomorphological changes in the upper GTR after gravel extraction led to critical changes in the hydrodynamics (as suggested by Jalón-Rojas et al., 2018), the impact of these hydrological changes on the TMZ occurred after the 1970s, when the tidal propagation from the lower Gironde pushed sediments into this area. Given the importance of the muddy soil boundary $x_{end,m}$ on the TMZ predictions, it would be worthwhile to calculate $x_{end,m}$ as a function of the suspended-sediment concentrations in future studies.

4.3. Model limitations

This model study is highly idealized and includes simplified representations of geometry, bed friction, eddy viscosity and, consequently, some physical processes. In particular, addition of a critical shear stress for erosion may change the timing of the sediment concentration (i.e. phase of the M2 and M4 components of concentration) relative to the flow, hence changing the transport related to tidal asymmetry.. Overall, we have demonstrated that the model was able to reproduce the longitudinal evolution of tidal parameters for various years and the distribution of suspended sediment concentration for recent scenarios, allowing for a systematic analysis of the main physical mechanisms and their variability over the decades.

It should be noted that the observed concentrations used in the calibration of the year 2014 includes values capped at 5g/L, which is the maximum concentration detected by the MAGEST turbidity sensor (Fig. 5.c). Even if the tidally-averaged concentration used to calibrate the model might be slighly underestimated during the period of very high concentration in the TMZ, it is at levels much higher than the threshold that indicates the occurrence of the TMZ. In addition, the lack of historical data hampered the calibration of the level of concentration for the rest of the years. Therefore, concentrations were scaled with the seaward concentration $c_{x=0}$ and results were interpreted in terms of spatial pattern of concentration without focusing on the magnitude. We would like to stress that historical river-discharge shifts could have an even greater impact on the observed concentration compared to the scaled concentration discussed here: the more frequent and higher floods before 1980s probably decreased the amount of available sediments in those years. Therefore, $c_{x=0}$ may have been significantly lower in 1953, resulting in the upper limit of the TMZ to be even more downstream for 1953 and 1971. A further more detailed study would be required to confirm this hypothesis.

4.4. Implications for other estuaries

This study is the first to encompass the effects of natural and anthropogenic geomorphological and hydrological changes on the long-term evolution of the TMZ. Evaluation of the individual effect of each pressure on each underlying physical mechanism is essential to understanding the long-term evolution of the system, but the potential feedback effects from the different pressures should also be considered. For example, the assessment of the impact of engineering activites (Winterwerp and Wang, 2013) but also of hydrological changes on SSC shifts should consider the concomitant changes in bottom roughness. In the Gironde fluvial-estuarine system, long-term hydrological and geomorphological changes are intrinsically related, and their feedback contributes to the intensification and upstream shift of the TMZ in the upper estuary. Nonetheless, pressures may lead to synergistic or antagonistic effects on sediment dynamics in other estuaries. For example, channel deepening decreased the level of sediment in the Scheldt estuary (Dijkstra et al., 2019a) while climate factors could have had contrasted effects. Even so, the conclusions of this work can serve as a reference for the assessment of natural and anthropogenic forcing on the sediment dynamics of similar hyperturbid estuaries (Mitchell, 2013). Forecasting studies show that the average discharges are projected to decrease in southern Europe, and extreme events to increase (Alfieri et al., 2015). Decreasing river flow is an important factor leading the natural evolution of the TMZ (Uncles et al., 2013), and therefore changes in morphology and bottom roughness. This implies that the intensification of the turbidity maximum in the upper GTR, and potentially in other neighboring macrotidal estuaries such as the Charente (Toublanc et al., 2016), the Loire (Jalón-Rojas et al., 2016) and the Seine (Grasso et al., 2019), is likely to increase further with the expected decrease in river flow over the next few decades.

5. Conclusions

We investigated the impact of climate and anthropogenic hydrogeomorphological changes on the sediment dynamics in the Garonne Tidal River (GTR), the upper region of the Gironde Estuary, using the idealized width-averaged iFlow model. A total of 20 scenarios were designed to reproduce the hydrodynamics and sediment transport during four morphological years (from the 1950s to the 2010s) with five different magnitudes of river discharge. The model

settings were adjusted to reflect the characteristics of the GTR and included some differences from previous applications of iFlow: (a) a landward non-reflecting boundary condition; (b) reference levels highly dependent on river flow; (c) tidal forcing dependent on the tidal characteristics at the open sea, the river discharge, and the year (to consider morphological changes downstream); and (d) bottom roughness varying spatially as a function of the type of bed, but also temporally with the year and the river discharge. The results should be interpreted qualitatively due to model schematizations and assumptions.

According to the simulations, all pressures affected the multi-decadal evolution of the TMZ but to different degrees. The geomorphological changes increased the SSC and gradually moved the upper limit of the TMZ upstream between 1953 and 2014; the turbidity maximum zone (TMZ) displacement was 7.5 km between these years for low river discharges. If the hydrological changes between these years are also considered (mean river discharge of 200 m^3/s and 140 m^3/s during the 1950s and 2010s, respectively) the upper boundary of the TMZ was displaced by 17 km in that period (by 4–8 km due to hydrological pressures). However, the lack of historical turbidity data hampered an accurate analysis of the impact of long-term hydrological trends on the absolute value of the sediment concentration and therefore a more accurate prediction of the historical TMZ shift.

Regarding the geomorphological changes, the natural evolution of the morphology in the lower Gironde Estuary is a key pressure impacting the evolution of the TMZ over the last six decades. These changes gradually increased tides, the flood dominance, and the landward transport capacity, leading to a more upstream and more concentrated TMZ. The other pressures also had an effect but to a lesser extent. The deepening of the GTR during the 1960s and the upstream shift of muddy beds might have contributed to the upstream shift of the TMZ because of an increase in the locally generated M_4 tide and thus the sediment advection and tidal return flow transport capacity in the upper GTR. However, the major effects on the TMZ probably took place from the 1970s, when tidal changes due to morphological changes in the lower Gironde pushed the TMZ up to this region.

Acknowledgments and Data

IJR acknowledges the Agence de l'Eau Adour-Garonne (AEAG) and the Aquitaine Region for financial support of her PhD research, and the LABEX COTE of the University of Bordeaux for a mobility grant to TU Delft. The authors thank Peter McIntyre for editorial help and Bas van Maren and an anonymous reviewer for their constructive reviews of this work. Water-level data were produced by the Bordeaux Harbour Authority, and are available at http://www.seanoe.org/data/00417/52798/. The iFlow model used for this study, together with a tutorial and a basic input file, is available for v2.5 on GitHub (doi: 10.5281/zenodo.822394) under an LGPL licence.

Appendix A. Formal definition of the transport capacity

The transport capacity T is the sediment transport that occurs when there is an abundance of sediment on the bed everywhere in the estuary. It can be defined from the sediment transport τ, which is written as the sum of the advetive and diffusive transport integrated over the cross-section:

$$\tau = \langle B \int_{-H}^{R+\zeta} uc - K_h c_x \mathrm{d}z \rangle$$

where B is the width, H is the bed level, R is the reference surface level, ζ is the surface elevation, u is the alon-channel velocity, c is the sediment concentration, c_x is the along-channel secdiment concentration gradient, and K_h is the horizontal eddy diffusivity.

This expression is rewrittng using iFlow's approximation of the sediment concentration (see Dijkstra et al., 2017 and Brouwer et al., 2018):

$$c = \hat{c}^f \, f + \, \hat{c}^{f_x} \, f_x$$

Here f is the erodibility, which is a measure between 0 and 1 of the abundance of sediment available at the bed for erosion. The quantity $\hat{c}^f$ is the sediment concentration suspended at capacity conditions. The term *capacity conditions* indicates the maximum concentration that can be supported by the flow, assuming an abundant availability of sediment. According to equation (A2), the concentration c equals $\hat{c}^f$ if there is an abundance of sediment, i.e. $f = 1$ everywehere (resulting in $f_x = 0$). The quantity represents the along-channel sediment dispersion by tidal advection at capacity conditions. The sediment transport equation can be rewritten by combining equations (A1) and A2):

$$\tau = \langle B \int_{-H}^{R+\zeta} \left(u\hat{c}^f - K_h \hat{c}_x^f\right) f - \left(\hat{c}^{f_x} + K_h \hat{c}^f\right) f_x \, \mathrm{d}z \rangle$$

The transport capacity T is defined as the first term divided by f:

$$T = \langle B \int_{-H}^{R+\zeta} u\hat{c}^f - K_h \hat{c}_x^f \mathrm{d}z \rangle$$

References

Alfieri, L., Burek, P., Feyen, L., & Forzieri, G. (2015). Global warming increases the frequency of river floods in Europe, *Hydrol. Earth Syst. Sci.*, 19, 2247–2260, doi:10.5194/hess-19-2247-2015.

Allen, G. P., Salomon, J. C., Bassoullet, P., Du Penhoat, Y., & De Grandpré, C. (1980). Effects of tides on mixing and suspended sediment transport in macrotidal estuaries. *Sedimentary Geology*, *26*, 69–90.

ARTELIA, IDRA, & ADICT. (2016). *Elaboration du plan de gestion des sédiments de dragage de l'estuaire de la Gironde*. Technical Repport.

Boé, J., Terray, L., Martin, E., & Habets, F. (2009). Projected changes in components of the hydrological cycle in French river basins during the 21st century. *Water Resources Research*, *45*(8), W08426. https://doi.org/10.1029/2008WR007437

Bonneton, P., Bonneton, N., Parisot, J.-P., & Castelle, B. (2015). Tidal bore dynamics in funnel-shaped estuaries. *Journal of Geophysical Research - Oceans*, *120*, 923–941.

Brouwer, R. L., Schramkowski, G. P., Dijkstra, Y. M., & Schuttelaars, H. M. (2018). Time evolution of estuarine turbidity maxima in well-mixed, tidally dominated estuaries: The role of availability- and Erosion-Limited conditions. *Journal of Physical Oceanography*, *48*, 1629'1650. https://doi.org/10.1175/JPO-D-17-0183.1

Burchard, H., Schuttelaars, H.M., Ralston, D.K. (2018). Sediment Trapping in Estuaries. *Annual Review of Marine Science, 10(1)*, 371–395.

Cai, H., Savenije, H. H. G., & Toffolon, M. (2012). A new analytical framework for assessing the effect of sea-level rise and dredging on tidal damping in estuaries. *Journal of Geophysical Research: Oceans*, *117*(9). https://doi.org/10.1029/2012JC008000

Castaing, P., Etcheber, H., Sottolichio, A., & Cappe, R. (2006). *Evaluation de l'évolution hydrologique et sédimentaire du système Garonne-Dordogne-Gironde*.

Chanson, H., Reungoat, D., Simon, B., & Lubin, P. (2011). High-frequency turbulence and suspended sediment concentration measurements in the Garonne River tidal bore. *Estuarine, Coastal and Shelf Science*, *95*(2–3), 298–306. https://doi.org/10.1016/j.ecss.2011.09.012

Cheng, Z., Jalón-Rojas, I., Wang, X.H., & Liu, Y. (2020). Impacts of land reclamation on sediment transport and sedimentary environment in a macro-tidal estuary, *Estuar. Coast. Shelf Sci.*, 221, 106861. https://doi.org/10.1016/j.ecss.2020.106861.

Chernetsky, A. S., Schuttelaars, H. M., & Talke, S. A. (2010). The effect of tidal asymmetry and temporal settling lag on sediment trapping in tidal estuaries. *Ocean Dynamics*, *60*(5), 1219–1241. https://doi.org/10.1007/s10236-010-0329-8

Costa, S., Picado, A., Vaz, N., Coelho, C., Portela, L., & Dias, J. M. (2018). Climate change effects on suspended sediment dynamics in a coastal lagoon: Ria de Aveiro (Portugal). *Proceedings from the International Coastal Symposium (ICS) 2018 (Busan, Republic of Korea). Journal of Coastal Research*, *85*, 521–525.

de Jonge, V. N., Schuttelaars, H. M., van Beusekom, J. E. E., Talke, S. A., & De-Swart, H. E. (2014). The influence of channel deepening on estuarine turbidity levels and dynamics, as exemplified by the Ems estuary. *Estuarine, Coastal and Shelf Science*, *139*, 46–59. https://doi.org/10.1016/j.ecss.2013.12.030

Dijkstra, Y. M., Brouwer, R. L., Schuttelaars, H. M., & Schramkowski, G. P. (2017). The iFlow modelling framework v2.4: A modular idealized process-based model for flow and transport in estuaries. *Geoscientific Model Development*, *10*, 2691–2713. https://doi.org/10.5194/gmd-10-2691-2017

Dijkstra, Y. M., Schuttelaars, H. M., & Schramkowski, G. P. (2019a). Can the Scheldt River Estuary become hyperturbid?: A model analysis of suspended sediment concentrations and

transport in response to channel deepening. *Ocean Dynamics*, *69*, 809–827. https://doi.org/10.1007/s10236-019-01277-z

Dijkstra, Y. M., Schuttelaars, H. M., & Schramkowski, G. P. (2019b). A Regime Shift From Low to High Sediment Concentrations in a Tide-Dominated Estuary. *Geophysical Research Letters*, *124*(3), 1578–1594. https://doi.org/10.1029/2019GL082302

Dijkstra, Y. M., Schuttelaars, H. M., Schramkowski, G. P., & Brouwer, R. L. (2019c). Modeling the Transition to High Sediment Concentrations as a Response to Channel Deepening in the Ems River Estuary. *Journal of Geophysical Research: Oceans*. https://doi.org/10.1029/2018JC014367

Etcheber, H., Schmidt, S., Sottolichio, A., Maneux, E., Chabaux, G., Escalier, J. M., Wennekes, H., Derriennic, H., Schmeltz, M., Quéméner, L., Repecaud, M., Woerther, P., & Castaing, P. (2011). Monitoring water quality in estuarine environments: lessons from the MAGEST monitoring programme in the Gironde fluvial-estuarine system. *Hydrology and Earth System Sciences*, *15*, 831–840. https://doi.org/10.5194/hess-15-831-2011

Familkhalili, R., & Talke, S. A. (2016). The effect of channel deepening on tides and storm surge: A case study of Wilmington, NC. *Geophysical Research Letters*, *43*(17), 9138–9147.

Fort, A., Jalón-Rojas, I., Hanquiez, V., Sottolichio, A., & Schmidt, S. (2018). Historical water level data in the Gironde Estuary. *SEANOE*. https://doi.org/https://doi.org/10.17882/52798

Friedrichs C.T. (2012). Tidal flat Morphodynamics: a synthesis. In: treatise on estuarine and coastal science. Estuarine and coastal geology and geomorphology, vol 3. Academic Press, Cambrige)

Friedrichs, C. T., & Aubrey, D. G. (1988). Non-linear tidal distortion in shallow well-mixed estuaries: a synthesis. *Estuarine, Coastal and Shelf Science*, *27*(5), 521–545. https://doi.org/10.1016/0272-7714(88)90082-0

Gallop, S. L., Collins, M., Pattiaratchi, C. B., Eliot, M. J., Bosserelle, C., Ghisalberti, M., Collins, L. B., Eliot, I., Erftemeijer, P. L. A., Larcombe, P., Marigómez, I., Stul, T., & White, D. J. (2015). Challenges in transferring knowledge between scales in coastal sediment dynamics. *Frontiers in Marine Science*, *2*, 82. https://doi.org/10.3389/fmars.2015.00082

Gibbs, R.J., Tshudy, D.M., Konwar, L., & Martin, J.M. (1989). Coagulation and transport of sediments in the Gironde Estuary. Sedimentology, 36, 987-999.

Grasso, F., & Le Hir, P. (2019). Influence of morphological changes on suspended sediment dynamics in a macrotidal estuary: diachronic analysis in the Seine Estuary (France) from 1960 to 2010. Ocean Dynamics, 69, 83–100.

Godin, G. (1999). The Propagation of Tides up Rivers With Special Considerations on the Upper Saint Lawrence River. *Estuarine, Coastal and Shelf Science*, *48*(3), 307–324. https://doi.org/10.1006/ecss.1998.0422

Guo, L., Van-der-Wegen, M., Jay, D. A., Matte, P., Wang, Z. B., Roelvink, D., & He, Q. (2015). River-tide dynamics: Exploration of nonstationary and nonlinear tidal behavior in the Yangtze River estuary. *Journal of Geophysical Research - Oceans*, *120*, 3499–3521. https://doi.org/10.1002/2014JC010491

Guo, W., Wang, X. H., Ding, P., Ge, J., & Song, D. (2018). A system shift in tidal choking due to the construction of Yangshan Harbour, Shanghai, China. *Estuarine, Coastal and Shelf Science*. https://doi.org/10.1016/j.ecss.2017.03.017

Jalón-Rojas, I., Sottolichio, A., Hanquiez, V., Fort, A., & Schmidt, S. (2018). To what extent multidecadal changes in morphology and fluvial discharge impact tide in a convergent (turbid) tidal river. *Journal of Geophysical Research: Oceans*, *123*(5), 3241–3258. https://doi.org/10.1002/2017JC013466

Jalón-Rojas, I., Schmidt, S., & Sottolichio, A. (2015). Turbidity in the fluvial Gironde Estuary (southwest France) based on 10-year continuous monitoring: sensitivity to hydrological conditions. *Hydrology and Earth System Sciences*, *19*, 2805–2819. https://doi.org/10.5194/hess-19-2805-2015

Jalón-Rojas, I., Schmidt, S., & Sottolichio, A. (2016a). Evaluation of spectral methods for high-frequency multiannual time series in coastal transitional waters: advantages of combined analyses. *Limnology and Oceanography: Methods*, *14*(6), 381–396.

Jalón-Rojas, I., Schmidt, S., Sottolichio, A., & Bertier, C. (2016). Tracking the turbidity maximum zone in the Loire Estuary (France) based on a long-term, high-resolution and high-frequency monitoring network. *Cont. Shelf Res.*, 117, 1-11.

Jalón-Rojas, I., Schmidt, S., & Sottolichio, A. (2017). Comparison of environmental forcings affecting suspended sediments variability in two macrotidal, highly-turbid estuaries. *Estuarine, Coastal and Shelf Science*, *198*, 529–541.

Jay, D. A., Leffler, K., & Degens, S. (2011). Long-Term Evolution of Columbia River Tides. *Journal of Waterway, Port, Coastal, and Ocean Engineering*, *137*(4), 182–191. https://doi.org/10.1061/(ASCE)WW.1943-5460.0000082

Little, S., Spencer, K. L., Schuttelaars, H. M., Millward, G. E., & Elliott, M. (2017). Unbounded boundaries and shifting baselines: Estuaries and coastal seas in a rapidly changing world. *Estuarine, Coastal and Shelf Science*, *198*, 311–319. https://doi.org/10.1016/j.ecss.2017.10.010

Manning, A. J., Dyer, K. R., Lafite, R., & Mikes, D. (2004). Flocculation measured by video based instruments in the Gironde estuary during the European commission SWAMIEE Project. *Journal of Coastal Research*, *41*(41), 59–69. http://www.jstor.org/stable/25736631

Mitchell, S. (2013). Turbidity maxima in four macrotidal estuaries, *Ocean and Coastal Management*,79, 62-69.

Moore, R. D., Wolf, J., Souza, A. J., & Flint, S. S. (2009). Morphological evolution of the Dee Estuary, Eastern Irish Sea, UK: A tidal asymmetry approach. *Geomorphology*, *103*(4), 588–596. https://doi.org/10.1016/j.geomorph.2008.08.003

Ralston, D. K., & Geyer, W. R. (2019). Response to channel deepening of the salinity intrusion, estuarine circulation, and stratification in an urbanized estuary. Journal of Geophysical Research: Oceans, 124, 4784– 4802.

Ralston, D. K., Talke, S., Geyer, W. R., Al- Zubaidi, H. A. M., & Sommerfield, C. K. (2019). Bigger tides, less flooding: Effects of dredging on barotropic dynamics in a highly modified estuary. Journal of Geophysical Research: Oceans, 124, 196– 211.

Ross, L., & Sottolichio, A. (2016). Subtidal variability of sea level in a macrotidal and convergent estuary. *Continental Shelf Research*, *131*(November), 28–41. https://doi.org/10.1016/j.csr.2016.11.005

Ross, L., Valle-Levinson, A., Sottolichio, A., & Huybrechts, N. (2017). Lateral variability of subtidal flow at the mid-reaches of a macrotidal estuary. *Journal of Geophysical Research: Oceans*, *122*(9), 7651–7673. https://doi.org/10.1002/2016JC012504

Savenije, H. H. G., Toffolon, M., Haas, J., & Veling, E. J. M. (2008). Analytical description of tidal dynamics in convergent estuaries. *Journal of Geophysical Research: Oceans*, *113*(10), 1–18. https://doi.org/10.1029/2007JC004408

Schuttelaars, H. M., de Jonge, V. N., & Chernetsky, A. (2013). Improving the predictive power when modelling physical effects of human interventions in estuarine systems. *Ocean & Coastal Management*, *79*, 70–82. https://doi.org/10.1016/j.ocecoaman.2012.05.009

Sottolichio, A., Hanquiez, V., Périnotto, H., Sabouraud, L., & Weber, O. (2013). Evaluation of the recent morphological evolution of the Gironde estuary through the use of some preliminary synthetic indicators. *Journal of Coastal Research*, *65*, 1224–1229. https://doi.org/10.2112/SI65-207.1

Talke, S. A., & Jay, D. A. (2020). Changing Tides: The Role of Natural and Anthropogenic Factors. *Annual Review of Marine Science*, *25*, 121–151. https://doi.org/10.1146/annurev-marine-010419-010727

Toublanc, F., Brenon, I, Coulombier, T. (2016). Formation and structure of the turbidity maximum in themacrotidal Charente estuary (France): Influence of fluvial and tidal forcing. *Estuarine, Coastal and Shelf Science,* 169, pp.1 – 14.

Uncles, R. J., Stephens, J. A., & Harris, C. (2013). Towards predicting the influence of freshwater abstractions on the hydrodynamics and sediment transport of a small, strongly tidal estuary: The Devonshire Avon. *Ocean Coast. Manage*., 79, 83–96.

Van Kessel, T., Vanlede, J., Eleveld, M., & Van der Wal, D. (2008). Mud transport model for the Scheldt estuary in the framework of LTV.Tech. rep., Deltares, Flanders Hydraulics, IVM, NIOO.

van Maanen, B., & Sottolichio, A. (2018). Hydro- and sediment dynamics in the Gironde estuary (France): Sensitivity to seasonal variations in river inflow and sea level rise. *Continental Shelf Research*, *165*, 7–50. https://doi.org/10.1016/j.csr.2018.06.001

van Maren, D. S., Winterwerp, J. C., & Vroom, J. (2015). Fine sediment transport into the hyper-turbid lower Ems River: the role of channel deepening and sediment-induced drag reduction. *Ocean Dynamics*, *65*(4), 589–605. https://doi.org/10.1007/s10236-015-0821-2

Van Maren D.S., Oost, A.P., Wang, Z.B., Vos P.C. (2016). The effect of land reclamations and sediment extraction on the suspended sediment concentration in the Ems estuary. *Mar Geol 376*, 147–157.

Vautard, R., Yiou, P., & Ghil, M. (1992). Singular-spectrum analysis: A toolkit for short, noisy chaotic signals. *Physica D*, *58*, 95–126.

Winterwerp, J. C., & Wang, Z. B. (2013). Man-induced regime shifts in small estuaries-I: theory. *Ocean Dynamics*, *63*(11–12), 1279–1292. https://doi.org/10.1007/s10236-013-0662-9

Winterwerp, J. C., Wang, Z. B., van Braeckel, A., van Holland, G., & Kösters, F. (2013). Man-induced regime shifts in small estuaries-II: a comparison of rivers. *Ocean Dynamics*, *63*(11–12), 1293–1306. https://doi.org/10.1007/s10236-013-0663-8